A Hybrid Filter Based Feature Selection, Segmentation and Ensemble Learning Model for Brain Stroke Prediction

Vijayadeep Gummadi^{1,3}, Dr. N. Naga Malleswara Rao²
Research Scholar, Department of Computer Science and Engineering¹
University College of Engineering, Acharya Nagarjuna University, Guntur, India
Professor and HoD, Department of CSE-IoT, RVR and JC College of Engineering(A), Guntur, India.²
Lecturer and HoD, Department of Computer Science³
SRR & CVR Govt. Degree College(A), Vijayawada, India

Abstract— Brain stroke detection (SD) is a critical medical task that can be effectively performed using magnetic resonance imaging (MRI). However, one of the major challenges in real-time systems is digital image denoising, as medical images often suffer from high noise levels and low resolutions. Noise arises from interand intra-signal variances during image acquisition, leading to significant degradation of image quality. Stroke-related MRI images are commonly affected by various types of noise, including Gaussian, speckle, impulsive, and mixed noise, which complicates reliable diagnosis.Traditional denoising methods-such as nonlinear median filters, Bayesian filters, wavelet-based shearlet transforms, non-local filters, and autoencoders—have been widely applied to reduce noise. Although these methods can handle specific noise types (e.g., speckle or Gaussian noise), their effectiveness is limited in medical imaging because of the simultaneous presence of additive, multiplicative, and Gaussian noise. Furthermore, the problem of sparsity in low signal-to-noise ratio (SNR) images remains unresolved with these conventional techniques, particularly in ultrasound and MRI-based stroke detection. To address these limitations, a hybrid non-linear filtering and segmentation-based ensemble learning framework is proposed. This approach enhances the denoising capability across different imaging modalities by leveraging the strengths of multiple techniques in a unified framework. Experimental results on real-time noisy images demonstrate that the proposed method outperforms conventional denoising approaches, thereby improving the reliability of stroke detection.

Index Terms— Brain stroke, feature extraction, stroke classification, machine learning models.

I. INTRODUCTION

Images play a fundamental role in human life and are an essential component of modern data processing. Digital **image processing** is employed to enhance the quality of the images, enabling computers to modify the image data for improved clarity, sharpness, and detail, thereby facilitating effective information extraction and analysis. Digital image processing, a subfield of signal processing, takes an

image as input and produces either a processed image or quantitative parameters that define specific features and operations (Cevik, 2011).

In many cases, noisy images are generated when a clean image is corrupted by external noise. **Image denoising**, the process of removing the noise component, has become a critical research area, with numerous techniques proposed, developed, and implemented over time. Advancements in technology have further increased the reliance on image acquisition and transmission as a preferred mode of information sharing, making efficient image processing indispensable.

Digital image processing serves two primary purposes: (i) improving the visual representation of an image for better human interpretation and (ii) enabling automated machine perception. Its applications are extensive, spanning medical imaging, biometrics, acoustic imaging, remote sensing and military surveillance. At its core, image processing involves applying computational operations to make the image content more meaningful and usable.

However, limitations in image sensors and transmission media often introduce **noise**, which manifests as signal disturbances that degrade image quality and hinder accurate monitoring, analysis, and evaluation. In such cases, image enhancement and restoration techniques are applied to recover the degraded or blurred images. Among these, **image denoising** is a critical step in image reconstruction algorithms,

supporting both direct photographic improvements and advanced technical applications.

A degraded image impairs automated processing and feature extraction, whereas a properly denoised image provides a reliable foundation for downstream tasks, such as biometric recognition, medical diagnostics, environmental monitoring, remote sensing, and defense applications. Thus, efficient image denoising remains central to the advancement of computer vision and intelligent image analysis.

As image acquisition devices evolve, their sensitivity to noise increases owing to the growing number of pixels per unit area. Consequently, **image denoising techniques** have become essential for minimizing the effects of noise and artifacts on image quality. Noise typically manifests as random fluctuations in pixel intensity or color values, arising from factors such as acquisition errors, quantization, transmission through noisy channels or environmental disturbances. Identifying the type of noise present in an image is often a prerequisite for applying suitable denoising algorithms.

A significant body of research in digital image processing is dedicated to denoising, including the development of novel algorithms and refinement of existing approaches under varying conditions. Because images can be corrupted during capture, transmission, or compression, denoising is a crucial step before any analytical or recognition tasks. **Image restoration** seeks to reduce the degradation caused by electronic and photometric noise, motion blur, and transmission errors. Among the many noise types, additive white Gaussian (AWG) noise, Poisson noise, thermal noise, salt-and-pepper noise, JPEG artifacts, and structured stripe noise are the most common. In this study, the focus is placed specifically on AWG noise.

Mathematical models based on **partial differential equations** (**PDEs**), including nonlinear diffusion and energy functional minimization, have been extensively explored. Earlier PDE-based models focused on speed control using smoothing operators or Laplacian-based formulations, whereas later approaches introduced coupled nonlinear diffusion equations to refine the control functions. The **Total Variation** (**TV**) **method** has also been influential in introducing a dynamic regularization framework. Variants include the Split Bregman iteration for the TV-ROF model, multiplicative regularization schemes for deblurring, and adaptive diffusion methods using local variance measures. Other models differentiate between noise-corrupted and noise-free pixels to achieve more selective denoising.

In addition to PDE-based methods, the **Discrete Wavelet Transform (DWT)** is widely employed for image denoising, particularly in applications such as texture analysis, object recognition, and segmentation. Recently, more advanced approaches have emerged, including **Non-Local Means (NLM)** and PCA-based adaptive filters, which improve precision. For example, PCA has been leveraged to derive surrogate

respiratory signals from single-lead ECGs to enhance the morphological analysis.

Traditional imaging systems also face challenges in effective signal processing due to increasing data complexity and limited computational resources. **Compressive sensing (CS)** has been introduced as an efficient alternative that reconstructs original signals from fewer measurements than Nyquist sampling. CS has proven especially useful in medical imaging modalities such as MRI, ultrasound, and CT, which are prone to random noise owing to radiation exposure. In particular, CS has been effective in reducing impulse and Gaussian noise in **Synthetic Aperture Radar (SAR)** images.

Overall, image denoising remains a critical research domain involving preprocessing, segmentation, classification, and parameter estimation to restore clean signals. Although numerous algorithms have been proposed, optimization challenges persist in achieving robustness against noise, scale, and variation in viewpoints. Denoising strategies can be broadly categorized into **thresholding**- and **segmentation-based** approaches. Thresholding separates image values into desired and undesired regions using an optimal threshold, whereas segmentation-based methods rely on the structural and contextual features of image regions.

Figure 1 illustrates the general workflow of image reconstruction, where filtering techniques are applied to suppress noise and enhance the brightness of high-resolution images. Effective denoising not only improves image quality but also provides a reliable foundation for subsequent tasks in medical imaging, remote sensing, biometrics and defence applications.

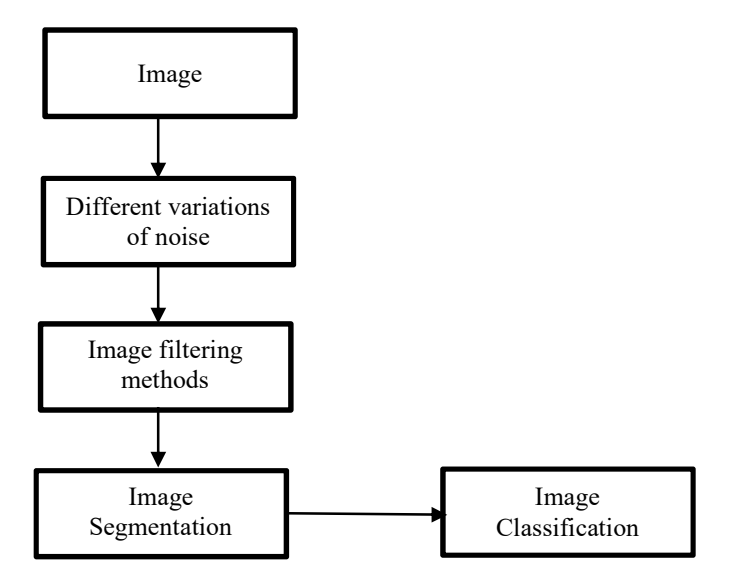


Figure 1: Segmentation-based image denoising

II. LITERATURE SURVEY

In this study, a novel image denoising approach is proposed that integrates wavelet transformation with optimized thresholding functions to effectively suppress noise. Wavelet threshold Denoising exhibits enhanced effectiveness relative to conventional methods, including Universal, SureShrink, and BayesShrink. Among the existing methods, BayesShrink produces outputs closest to high-quality images with minimal blurring, whereas VisuShrink and Universal methods perform poorly in handling salt-and-pepper noise.

The proposed method improves the denoising results by combining wavelet-based decomposition with advanced threshold selection. Because the choice of threshold is critical in wavelet-based denoising, this study introduces an **adaptive thresholding strategy** that leverages the spatial context modeling of wavelet coefficients for more accurate noise suppression. Experimental evaluations on multiple natural images indicate that the proposed technique significantly

Universal Denoising Algorithm:

- Step 1: Apply the wavelet transform to the noisy image.
- Step 2: Calculate the threshold value using the universal threshold formula, which is based on the wavelet coefficients' spatial context modeling.
- Step 3: Apply the thresholding function to the wavelet coefficients, setting all coefficients below the threshold to zero.
- Step 4: Apply the inverse wavelet transform to the thresholded coefficients to obtain the denoised image.

Sure Shrink Denoising Algorithm:

- Step 1: Apply the wavelet transform to the noisy image.
- Step 2: Calculate the threshold value using the sure shrink formula, which is based on the standard deviation of the wavelet coefficients.
- Step 3: Apply the thresholding function to the wavelet coefficients, setting all coefficients below the threshold to zero.
- Step 4: Apply the inverse wavelet transform to the thresholded coefficients to obtain the denoised image.

Bayes Shrink Denoising Algorithm:

- Step 1: Apply the wavelet transform to the noisy image.
- Step 2: Calculate the threshold value using the Bayes shrink formula, which is based on the prior probability distribution of the wavelet coefficients.
- Step 3: Apply the thresholding function to the wavelet coefficients, setting all coefficients below the threshold to
- Step 4: Apply the inverse wavelet transform to the thresholded coefficients to obtain the denoised image.

outperforms conventional PCA-based methods, delivering higher visual quality and robustness for different noise types.

Furthermore, a **multivariate statistical method** was introduced for denoising multispectral images in the wavelet domain by leveraging the correlations among different spectral components. To achieve this, the application of the recently developed **hyperanalytic wavelet transform (DWT)** has been suggested [15–18].

The proposed algorithm for image denoising utilizes a combination of wavelet transformation and optimized thresholding functions, resulting in a fast and effective noise removal method. The simulation results and comparisons show that the performance of the proposed method is superior to that of previous thresholding methods. Additionally, an iterative image reconstruction technique using the Maximum Likelihood Expectation Maximization wavelet-based thresholds (EM) was proposed to overcome the difficulties associated with large amounts of data and noise in Compton scatter camera data. This method leads to less reconstruction errors than other algorithms

Initialize the wavelet coefficients of the noisy image and the noise standard deviation for each sub-band.

Perform the Expectation step:

Estimate the probability that each wavelet coefficient belongs to the noise or signal class. Update the noise standard deviation for each sub-band based on the estimated probability. Perform the Maximization step:

Update the wavelet coefficients of the denoised image based on the estimated probability and the noise standard deviation

Repeat steps 2 and 3 until convergence, or a set number of iterations is reached. Perform the inverse wavelet transform to obtain the denoised image.

such as MLEM and Gaussian smoothing, and is also stable. Another method proposed in the literature is the amendment of the projection operation in existing Principal Component Analysis (PCA) kernel denoising algorithms in order to avoid poor denoising results caused by geometric arguments[19-20].

Estimating multidimensional probability density functions (PDFs) is a challenging task in signal processing. To address this, [21] introduced an **iterative Gaussianizing rotational family**, which applies marginal transformations for univariate Gaussianization, followed by orthonormal transformations, thereby simplifying PDF estimation.

Wavelet-based thresholding methods have also attracted significant attention. As suggested in [22], these methods outperform conventional approaches; however, threshold estimation and selection remain difficult. To overcome this, a **new continuous high-order threshold function** is proposed, making it suitable for gradient-based techniques, such as neural

thresholds (TNN). Within this framework, the **Least Mean Square (LMS) algorithm** is employed to estimate the threshold values for the **wavelet subband coefficients**. Beyond conventional hard and soft threshold operators, semi-soft and Stein thresholding are also evaluated in the shrinkage step, particularly for medical image denoising across various wavelet families. Experimental results on textured and satellite images, measured using PSNR and classification accuracy, demonstrate that **anisotropic distributions** yield effective denoising performance.

Complementary approaches have been proposed for image denoising using partial differential equations (PDEs) [23]. Three PDE-based techniques were compared using metrics such as the average absolute difference, SNR, PSNR, image fidelity, and MSE. The results confirm their superiority over traditional techniques. Furthermore, the use of **bi-dimensional empirical mode decomposition (BEMD)** was explored, with theoretical insights validating its numerical performance in digital image denoising.

Edge preservation is another critical issue in denoising. In [24], a directional denoising system with an integrated directional interpolator was proposed to mitigate structural distortions that typically occur at image edges during denoising. Similarly, [25] enhances the Singular Value Decomposition (SVD) framework by embedding it within a filter bank structure. This advancement facilitates the design of anti-forensic techniques aimed at eliminating compression fingerprints, specifically targeting JPEG and wavelet-based artifacts.

Machine learning has also been used for image denoising and classification. Feature extraction is often performed using **Gabor filters** to capture local edges and texture patterns, whereas classification is enhanced using the **AdaBoost algorithm**, which combines multiple weak classifiers to improve decision accuracy. Performance evaluations before and after boosting demonstrated notable improvements, particularly in the classification of **stroke tissue images**, underscoring the effectiveness of ensemble-based machine learning in medical image analysis.

The remainder of this paper is structured as follows: Section 2 presents the hybrid stroke detection framework, focusing on feature extraction and the classification models. Section 3 discusses the simulation results of the stroke prediction model and its performance metrics. Finally, Section 4 concludes the paper and highlights the observed performance improvements of the proposed method.

III. PROPOSED MODEL

A very important aspect of image analysis is texture, which is usually utilized to recognize objects or areas of interest. One widely employed statistical technique of texture analysis is the gray-level co-occurrence matrix (GLCM), or gray spatial dependency matrix.

The GLCM captures the spatial relationship between pixels by quantifying how often pairs of pixels with specific intensity values occur in an image. Various statistical descriptors can be extracted from this matrix to represent the texture.

Formally, let FFF be a rectangular discrete image with a finite number of gray levels defined over a given domain. The extracted texture features should not only describe image patterns but also relate to clinical aspects, such as disease progression and its impact on patient outcomes. For instance, the consistency of the association between extracted features and stroke occurrence can be assessed, as well as their correlation with outcomes such as hospitalization or mortality.

A crucial consideration is whether these features can be influenced or modified by medical interventions. Controlled trials and randomized studies provide evidence of whether changes in feature status translate into meaningful clinical outcomes, including survival. It is also essential to determine whether the extracted features capture short- or long-term effects and to scientifically validate whether such variations significantly affect prognosis.

Unlike natural objects, **lesions in medical images often lack a consistent shape**, rendering shape-based features less reliable. Instead, texture is a dominant factor, as medical images are typically rich in textural details. Although local regions may appear irregular, the overall image often exhibits a certain degree of regularity, commonly referred to as *texture*. Consequently, texture analysis plays a vital role in the effective interpretation and recovery of information from medical images.

Non-linear Filtering approach

In data filtering algorithm, sensitive attributes specific to the user are added to the filtering process. To provide privacy, probabilistic noise was added to these attributes and a perturbed dataset was obtained to use in the mean clustering stage. In the hybrid perturbed mean clustering algorithm, new perturbed data clustered classes are generated using kkk representative centers and a weighting measure. The privacy-preserving classification was subsequently done using the resulting kkk-clustered training data. Lastly, ensemble classification model was used to predict the test samples using the clustered training data.

Algorithm1: Data filtering algorithm

Algorithm 1: Algorithm 1 outlines the filtering process applied to a large input dataset for mean clustering with privacy preservation. In Steps 1 and 2, the input dataset, along with its sensitive attributes, is acquired. In Step 3, each sensitive attribute undergoes a transformation using sine and cosine measures. In Steps 5–8, additional privacy is ensured by applying probabilistic noise to sensitive attributes. Finally, a perturbed dataset was generated and prepared for the mean clustering process.

Input: Dataset DS, Features space SA.

Output: Perturbed transformed values PD.

Procedure:

Read input dataset DS

Read sensitive attributes SA from the input dataset DS. Transform sensitive attributes SA using sin and cos

measures as

$$DS' = v \cos(v)$$
 if i!=j

To each value in the sensitive attributes SA

Compute probability noise to the transformed sensitive attribute:

$$P_{N}(DS_{A}^{'}(v)) = \frac{2 \mid \max\{DS_{A}^{'}(v)\} \cdot e^{-\frac{(DS_{A}^{'}(v) - \mu_{DS_{A}^{'}(v)})}{\sigma_{DS_{A}^{'}(v)}^{2}}}}{v \cdot \cos(v) \cdot \sigma_{DS_{A}^{'}(v)}}; if i!=j$$

$$9. \quad P_{N}(DS_{A}^{'}(v)) = \frac{2 \mid \min\{DS_{A}^{'}(v)\} \cdot e^{-\frac{(DS_{A}^{'}(v) - \mu_{DS_{A}^{'}(v)})}{\sigma_{DS_{A}^{'}(v)}}}}{v \cdot \sin(v) \cdot \sigma_{DS_{A}^{'}(v)}}; if i=$$

Done

Final transformed perturbed dataset D is given as

 $PD=P_{N}(DS_{A}(v)) \cup DS$

Proposed Feature Extraction Measure: Log Inverse **Differential Moment (LIDM):**

The LIDM is employed to evaluate the **homogeneity of image** structures and serves as a discriminative feature for effective image classification.

Max Correlation Inertia: MCI

MCI is used to determine the maximal correlation between the gray-level linear dependence among pixels at given positions.

The Probabilistic Gray-Level Co-occurrence Matrix (PGLCM) algorithm computes probabilistic measurements of image texture based on the spatial relationships between pixels of the same gray level. The steps of the GLCM algorithm are as follows:

- Convert the image to a grayscale image if it is not already grayscale.
- The distance and direction parameters for the GLCM matrix are defined as follows: The distance parameter determines the number of pixels away from a given pixel that will be used to calculate the co-occurrence probability. The direction parameter determines the direction in which the co-occurrence probability is
- The GLCM matrix is initialized with zeros. The matrix has a size of $(L \times L)$, where L is the number of gray levels in the image.

- The algorithm iterates through each pixel in the image. For each pixel, the co-occurrence probability is calculated with the pixel that is at a specified distance and direction away. The co-occurrence probability is calculated as follows:
- P(i, j) = n(i, j) / (M * N)
- where n(i, j) is the number of occurrences of the pair of gray levels i and j, and M and N are the number of rows and columns in the image, respectively.
- The corresponding element in the GLCM matrix is incremented by the co-occurrence probability calculated in step 4.
- After iterating through all the pixels, the GLCM matrix is normalized by dividing each element by the sum of all elements in the matrix.
- The normalized GLCM matrix was used to calculate probabilistic measurements, such as energy, entropy, contrast, and homogeneity. These measurements were calculated using the following equations:
- Energy = $sum(P(i, j)^2)$
- Entropy = -1 * sum(P(i, j) * log(P(i, j)))
- $Contrast = sum((i j)^2 * P(i, j))$
- Homogeneity = $sum(P(i, j) / (1 + (i j)^2))$
- return the probabilistic measurements

Max Entropy Texture extraction measure: MEM

Statistical entropy measures the disorder or complexity of an image.

Non-linear Kernel Estimator: NLKE

NLKE is used to find the nonlinear structure of the image patterns using the Gaussian distribution measure.

The nonlinear kernel estimator (NLKE) algorithm is a technique used to estimate probability density functions (PDFs) in nonlinear, high-dimensional spaces. The algorithm is based on kernel functions to approximate the underlying PDF.

The main steps of the NLKE algorithm are as follows.

- Select a kernel function, k(x,y), which is used to approximate the underlying PDF. Common choices for kernel functions include the Gaussian and Epanechnikov kernels.
- A bandwidth parameter, h, which controls the width of the kernel function, is defined. A larger bandwidth leads to a smoother PDF estimate, whereas a smaller bandwidth results in a more detailed estimate.
- Estimate the density at each data point, x, by averaging the kernel function over all data points: f hat(x) = (1/nh) * Sum(k((x-x i)/h)) for i=1 to n

where n is the number of data points and x i is the i-th data point.

- Normalize the density estimate by dividing by the total sum of the density estimate: f hat(x) = f hat(x)/ Sum(f hat(x))
- Use the density estimate to calculate the probability of observing a new data point, x new, by evaluating the density estimate at x new: P(x new) = f hat(x new)
- Repeat steps 3-5 for different values of h to determine the optimal bandwidth parameter that results in the best PDF estimate.

Proposed Bayesian feature selection

The Bayesian probabilistic measure is evaluated using the following function:

The optimal compressive sensing reconstruction measure is computed using the following equation:

$$I_R = (1 + \lambda) \frac{\sigma_E^2}{\sqrt{Max(\sigma_0^2 - \sigma_E^2, 0)}}$$

 $B_f = uniCV(D); //Unique column values$

 $HB_f = Histobins[] = histogrambin(D)$

Gaussian Kernel:
$$GK(\phi, \theta) = e^{-\theta^2}/(2 * \log(\phi))$$

$$\psi = \text{gkv} = \text{GK}(\sum HB_f, 1/2\sum B_f);$$

Exponential Gaussian Probability = KP(D)

$$= \mid HB_{\rm f} / (\sum log(\psi) * HB_{\rm f}) \mid$$

PolyDiffusion = PD = KP(D).
$$-\frac{1}{2}\int (I_{Original}(i,j) - \frac{\partial^2 I_{Original}(i,j)}{\partial z^2})$$

$$\varphi_{noise}(i,j))^k dxdy + m.\frac{\partial^2 I_{original}(i,j)}{\partial X^2}$$

$$min\{R(X)\} = PD.\frac{1}{2} \|\sigma_0^2 - \sigma_E^2\|^2 + I_R.\emptyset(X)$$

Where, $\phi(x) \phi(x)$ represents the **non-linear** and non-smooth regularizer. The proposed iterative method is employed to solve R(x)R(x)R(x), enabling the restoration of the noisy input image with a high PSNR value and a low error rate.

Algorithm 2: hybrid filtering mean clustering algorithm

Input: Perturbed dataset PD

Output: Perturbed dataset with clustered class labels

Initialize k randomized centers Procedure: representative objects in the PD. Compute the mean perturbed measure using the following formula

$$\phi(PD) = min \left\{ \frac{\sum_{i=1}^{|N|} max\{PD_{A_i}\}}{\sum_{j=1}^{|R|} \frac{1}{|PD_{A_jr} - C_r|^p}} \right\}; r=1..|R|$$

Compute the filtering membership function using the following formula

$$P_m \left({\binom{C_j}{V_i}} \right) = \emptyset(PD) \cdot \frac{|V_i - c_j|^{-p-2}}{\sum_{j=1}^k |V_i - c_j|^{-p-2}}$$

$$P_m\binom{C_j}{V_i} = \emptyset(PD). \frac{|V_i - c_j|^{-(p+2)}}{\sum_{i=1}^k |V_i - c_i|^{-(p+2)}}$$

To each perturbed object, compute the weight of the object for membership update as

$$w_p(V_i) = \emptyset(PD) \cdot \frac{|V_i - c_j|^{-p-2}}{\left[\sum_{j=1}^k |V_i - c_j|^{-(p+2)}\right]^2}$$
 Updating the centroid location by using the

$$C_{j} = \frac{\sum_{i=1}^{n} P_{m} \binom{C_{j}}{V_{i}} . w_{p}(V_{i}) . V_{i}}{\sum_{j=1}^{n} P_{m} \binom{C_{j}}{V_{j}} . w_{p}(V_{i})}$$

Repeat the procedure till k clusters.

Assign each filtering object v_i to cluster j by using the highest membership value $P_m(C_i / v_i)$.

$$PD_c^{Tr} = P_m(C_i / v_i)$$

The algorithm 2 shows the mean clustering methodology to predict the class labels on the filtered dataset. In the first step, as representative objects in the perturbed dataset (PD), kkk randomized centers are identified. The \phivalue used to estimate membership is calculated using the mean perturbed measure in Step 2. Cluster memberships in Steps 4-6 are computed based on the proposed equation. Lastly, Steps 7-8 involves updating the weighted memberships (according to the calculated measures).

Algorithm 3: Input training and testing classification model

Input: Training data PD_c^{Tr} Procedure: To each instance in PD_c^{Tr} Do $\mu_i^p = PMean(PD_c^{Tr})$ $\sum_i = CovMat(PD_c^{Tr})$ $P_i = classify\left(Ens, \left(\mu_i^p, \sum_i^p\right)\right)$ Done To each test sample t in PD_c^{Tr} $\mu_i^p = PMean(PD_c^{Tr} \cup \{t\})$ $\sum_i^{p*} = CovMat(PD_c^{Tr} \cup \{t\})$ $P_i^* = classify\left(Ens, \left(\mu_i^{p*}, \sum_i^{p*}\right)\right)$ Find Δp_i using the (P_i, P_i^*) ass Euclidean norm Class(t) = $\operatorname{argmin}(\Delta p_i)$

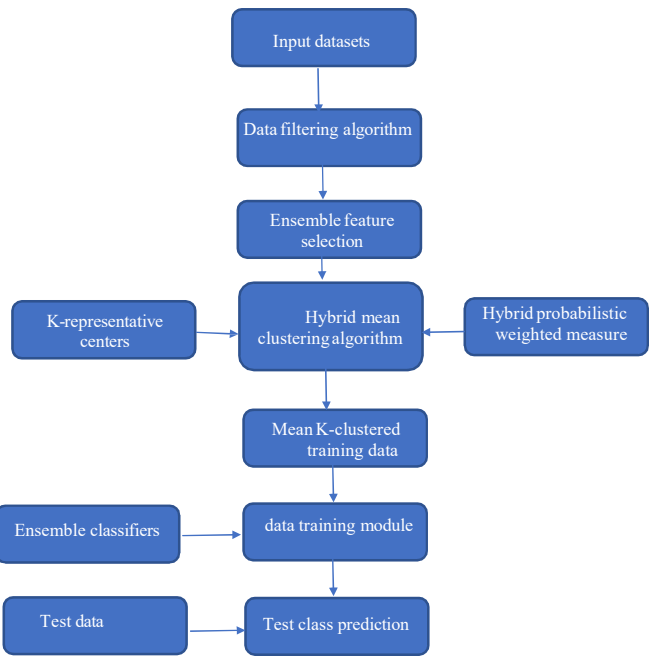


Figure 1: Proposed Model

The classification learning process of the proposed model with clustered learning dataset is described in Algorithm 3. Under this approach, mean, covariance, and ensemble learning

approaches are used to conduct the training and testing. The difference in the values of the delta between the predicted values is calculated by the Euclidean norm and the one with the smallest norm is taken as the final label of the classes.

In the proposed boosting system, a pool of weak classifiers is utilized in order to increase the overall classification rate. In particular, weak learners in the AdaBoost system are decision trees. Entropy- and conditional- entropy-based decision trees are optimized (improved) to enhance their performance by using a modified attribute ranking measure during construction. The classifier that has the lowest error rate in classification is eventually selected in predicting instances.

IV. EXPERIMENTAL RESULTS

Experimental evaluations were performed on multiple training datasets for **stroke disorder prediction**. To support this, a **new classification model** was developed and deployed on an **Amazon AWS server** with 20 GB RAM, enabling the prediction of novel disorder types. The experiments were conducted using the **Java programming environment**, with simulations performed on a dedicated **stroke image database**.

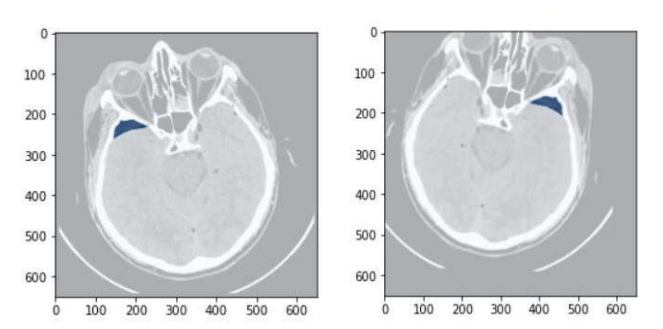


Figure 2: Sample stroke image

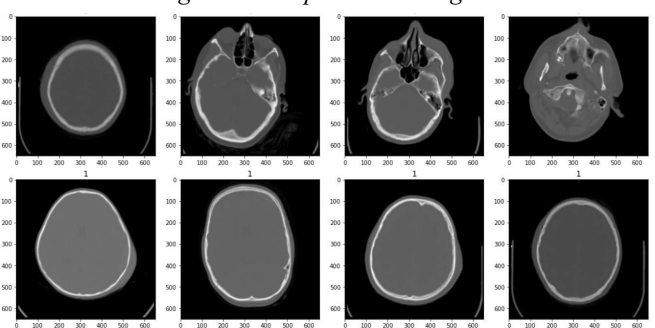


Figure 3: Comparative analysis of proposed model to the traditional techniques

Table 1, describes average PSNR ratio for all images with different types of noise levels.

A. T=0.75

Images	Line ar Filter	Non- Line ar Filter	Bayesi an Filter	Wavele tT Filter	Prob denoisi ng	Propos ed
SAR	4873	4409	4193	4099	3949	3408

DENTAL	4865	4511	4024	4407	4092	3356
Hyperspect ral	4863	4099	3962	3969	3990	3320

B T=0.8

Images	Line	Non-	Bayesi	Wavele	Prob	Propos
	ar	Line	an	tT Filter	denoisi	ed
	Filter	ar	Filter		ng	
		Filter				
SAR	4867	4138	4187	4223	4064	3285
DENTAL	4866	4508	3992	4124	3905	3375
Hyperspect	4836	4207	4050	4516	3964	3456
ral						

C. T=0.85

Images	Line	Non-	Bayesi	Wavele	Prob	Propos
	ar	Line	an	tT Filter	denoisi	ed
	Filter	ar	Filter		ng	
		Filter				
SAR	4836	4098	4144	4103	4168	3485
DENTAL	4865	4559	4172	4047	3892	3463
Hyperspect	4839	4836	4135	4266	4169	3481
ral						

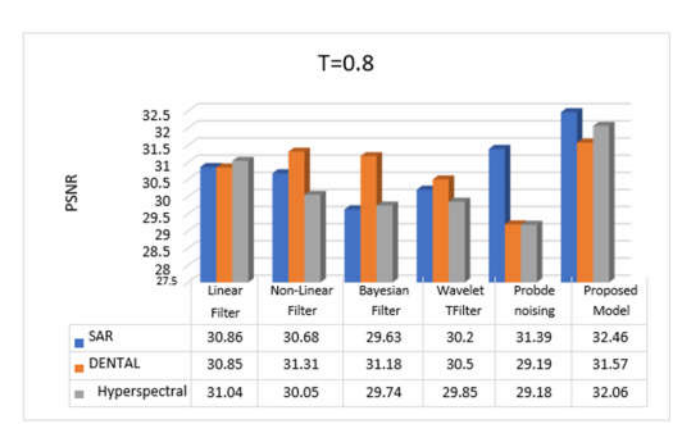


Figure 4: Comparative analysis of proposed model to the traditional techniques

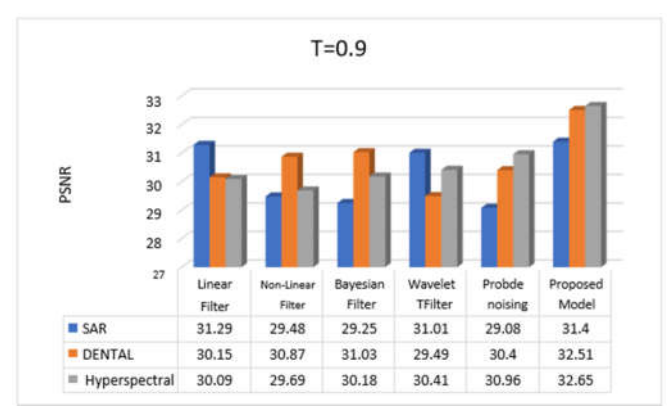


Figure 5: Comparative analysis of proposed model to the traditional techniques

V. CONCLUSION

Prediction of disease in the vertebral column dataset is a challenging task, primarily due to noise and feature selection issues in stroke disorder analysis. Identifying relational patterns among disc features is particularly difficult because of variations in disc parameters. Traditional filtering, segmentation, and classification models often treat image features independently, without considering their interrelationships in disc disorder characterization.

In order to deal with these shortcomings, a hybrid-threshold based image segmentation and classification model is suggested in order to predict disorder. The model combines a hybrid property selection process and a powerful decision tree classifier that is able to narrow important features to make correct predictions. The results of the experiments prove that the model is superior to the known techniques, and the model has high performance with the following values: TP rate = 0.979133, accuracy = 0.98233, and error rate = 0.0216, as well as F-measure and recall improvements.

For future work, an advanced feature selection-based classification learning approach will be explored to further enhance prediction accuracy in stroke detection.

REFERENCES

- [1] K. M. Poloni and R. J. Ferrari, "A deep ensemble hippocampal CNN model for brain age estimation applied to Alzheimer's diagnosis," Expert Systems with Applications, vol. 195, p. 116622, Jun. 2022, doi: 10.1016/j.eswa.2022.116622.
- [2] P. Kunwar and P. Choudhary, "A stacked ensemble model for automatic stroke prediction using only raw electrocardiogram," Intelligent Systems with Applications, vol. 17, p. 200165, Feb. 2023, doi: 10.1016/j.iswa.2022.200165.
- [3] A. Akyel, "Accurate estimation of stroke risk with fuzzy clustering and ensemble learning methods," Biomedical Signal Processing and Control, vol. 77, p. 103764, Aug. 2022, doi: 10.1016/j.bspc.2022.103764.
- [4] J. Emakhu et al., "Acute coronary syndrome prediction in emergency care: A machine learning approach," Computer Methods and Programs in Biomedicine, vol. 225, p. 107080, Oct. 2022, doi: 10.1016/j.cmpb.2022.107080.
- [5] L. Brunese, F. Mercaldo, A. Reginelli, and A. Santone, "An ensemble learning approach for brain cancer detection exploiting radiomic features," Computer Methods and Programs in Biomedicine, vol. 185, p. 105134, Mar. 2020, doi: 10.1016/j.cmpb.2019.105134.

- [6] F. Wang, Y.-C. Tian, X. Zhang, and F. Hu, "An ensemble of Xgboost models for detecting disorders of consciousness in brain injuries through EEG connectivity," Expert Systems with Applications, vol. 198, p. 116778, Jul. 2022, doi: 10.1016/j.eswa.2022.116778.
- [7] F. Guo, M. Ng, G. Kuling, and G. Wright, "Cardiac MRI segmentation with sparse annotations: Ensembling deep learning uncertainty and shape priors," Medical Image Analysis, vol. 81, p. 102532, Oct. 2022, doi: 10.1016/j.media.2022.102532.
- [8] A. Pinto et al., "Combining unsupervised and supervised learning for predicting the final stroke lesion," Medical Image Analysis, vol. 69, p. 101888, Apr. 2021, doi: 10.1016/j.media.2020.101888.
- [9] L. Guo, S. Kondapavulur, S. M. Lemke, S. J. Won, and K. Ganguly, "Coordinated increase of reliable cortical and striatal ensemble activations during recovery after stroke," Cell Reports, vol. 36, no. 2, p. 109370, Jul. 2021, doi: 10.1016/j.celrep.2021.109370.
- [10] K. R. M. Fernando and C. P. Tsokos, "Deep and statistical learning in biomedical imaging: State of the art in 3D MRI brain tumor segmentation," Information Fusion, vol. 92, pp. 450–465, Apr. 2023, doi: 10.1016/j.inffus.2022.12.013.
- [11] Z. Tang et al., "Deep Learning-Based Prediction of Hematoma Expansion Using a Single Brain Computed Tomographic Slice in Patients With Spontaneous Intracerebral Hemorrhages," World Neurosurgery, vol. 165, pp. e128–e136, Sep. 2022, doi: 10.1016/j.wneu.2022.05.109.
- [12] N. M. Wormi, B. I. Ya'u, S. Boukari, M. A. Musa, F. Shittu, and M. A. Lawal, "Deeper Architecture for Brain Age Prediction Based on MRI Images Using Transfer Learning Technique," Procedia Computer Science, vol. 212, pp. 441–453, Jan. 2022, doi: 10.1016/j.procs.2022.11.028.
- [13] H. Zhang et al., "Development and validation of comprehensive clinical outcome prediction models for acute ischaemic stroke in anterior circulation based on machine learning," Journal of Clinical Neuroscience, vol. 104, pp. 1–9, Oct. 2022, doi: 10.1016/j.jocn.2022.07.022.
- [14] S. K. Prabhakar and S.-W. Lee, "ENIC: Ensemble and Nature Inclined Classification with Sparse Depiction based Deep and Transfer Learning for Biosignal Classification," Applied Soft Computing, vol. 117, p. 108416, Mar. 2022, doi: 10.1016/j.asoc.2022.108416.
- [15] L. Zheng et al., "Ensemble learning method based on temporal, spatial features with multi-scale filter banks for motor imagery EEG classification," Biomedical

- Signal Processing and Control, vol. 76, p. 103634, Jul. 2022, doi: 10.1016/j.bspc.2022.103634.
- [16] S. Roy, U. Roy, D. Sinha, and R. K. Pal, "Imbalanced ensemble learning in determining Parkinson's disease using Keystroke dynamics," Expert Systems with Applications, vol. 217, p. 119522, May 2023, doi: 10.1016/j.eswa.2023.119522.
- [17] M. S. Sirsat, E. Fermé, and J. Câmara, "Machine Learning for Brain Stroke: A Review," Journal of Stroke and Cerebrovascular Diseases, vol. 29, no. 10, p. 105162, Oct. 2020, doi: 10.1016/j.jstrokecerebrovasdis.2020.105162.
- [18] H. Hoffman, J. S. Wood, J. R. Cote, M. S. Jalal, H. E. Masoud, and G. C. Gould, "Machine learning prediction of malignant middle cerebral artery infarction after mechanical thrombectomy for anterior circulation large vessel occlusion," Journal of Stroke and Cerebrovascular Diseases, vol. 32, no. 3, p. 106989, Mar. 2023, doi: 10.1016/j.jstrokecerebrovasdis.2023.106989.
- [19] R. Karthik, R. Menaka, A. Johnson, and S. Anand, "Neuroimaging and deep learning for brain stroke detection - A review of recent advancements and future prospects," Computer Methods and Programs in Biomedicine, vol. 197, p. 105728, Dec. 2020, doi: 10.1016/j.cmpb.2020.105728.
- [20] J. Zhou et al., "Predicting Stroke and Mortality in Mitral Regurgitation: A Machine Learning Approach," Current Problems in Cardiology, vol. 48, no. 2, p. 101464, Feb. 2023, doi: 10.1016/j.cpcardiol.2022.101464.
- [21] R. Huang et al., "Stroke mortality prediction based on ensemble learning and the combination of structured and textual data," Computers in Biology and Medicine, p. 106176, Oct. 2022, doi: 10.1016/j.compbiomed.2022.106176.
- [22] L. Schwartz, R. Anteby, E. Klang, and S. Soffer, "Stroke mortality prediction using machine learning: systematic review," Journal of the Neurological Sciences, vol. 444, p. 120529, Jan. 2023, doi: 10.1016/j.jns.2022.120529.
- [23] R. Raj, J. Mathew, S. K. Kannath, and J. Rajan, "StrokeViT with AutoML for brain stroke classification," Engineering Applications of Artificial Intelligence, vol. 119, p. 105772, Mar. 2023, doi: 10.1016/j.engappai.2022.105772.
- [24] A. Peters, M. Sprengell, and B. Kubera, "The principle of 'brain energy on demand' and its predictive power for stress, sleep, stroke, obesity and diabetes," Neuroscience & Biobehavioral Reviews, vol. 141, p. 104847, Oct. 2022, doi: 10.1016/j.neubiorev.2022.104847.

[25] S. M. Hofmann et al., "Towards the interpretability of deep learning models for multi-modal neuroimaging: Finding structural changes of the ageing brain," NeuroImage, vol. 261, p. 119504, Nov. 2022, doi: 10.1016/j.neuroimage.2022.119504.